ULTRA SONO GRAPHY

Diagnostic performance of vector flow imaging–derived wall shear stress and radiofrequency echo-tracking–derived arterial stiffness indices in severe carotid stenosis

Nezih Yaylı[1], Atiye Cenay Karabörk Kılıç[2], Burcu Küçük Biçer[3], Fatih Öncü[2], Taylan Altıparmak[4], Mahi Nur Cerit[2], Halit Nahit Şendur[2], Hale Zeynep Batur Çağlayan[4], Mehmet Koray Akkan[2], Hüseyin Koray Kılıç[2], Suna Özhan Oktar[2], Ahmet Baran Önal[2], Bijen Nazlıel[4], Erhan Turgut Ilgıt[2]

[1]Department of Radiology, Bozok University Faculty of Medicine, Yozgat; [2]Department of Radiology, Gazi University Faculty of Medicine, Ankara; [3]Department of Medical Education and Informatics, Gazi University Faculty of Medicine, Ankara; [4]Department of Neurology, Gazi University Faculty of Medicine, Ankara, Türkiye

Purpose: This study aimed to evaluate the diagnostic performance of vector flow imaging (VFI)–derived hemodynamic parameters and radiofrequency echo-tracking–derived arterial stiffness indices (RF-ASI) for detecting severe carotid artery stenosis.

Methods: This prospective, single-center observational study included 90 patients with carotid artery disease examined between May and July 2024. Stenosis severity was categorized as <50%, 50%–69%, and ≥70% according to the Society of Radiologists in Ultrasound (SRU) Doppler criteria. In patients with stenosis ≥50%, severity was confirmed using digital subtraction angiography, computed tomography angiography, or magnetic resonance angiography. At the plaque level, VFI-derived wall shear stress (WSS) and turbulence metrics, as well as RF-ASI, were measured. Correlation analyses, group comparisons, and receiver operating characteristic analysis were performed to evaluate each parameter's ability to detect ≥70% stenosis.

Results: Among the 90 patients (mean age, 70.4±8.7 years; 55.6% male), peak-segment mean wall shear stress (WSSmean) demonstrated the strongest correlation with stenosis severity (r_s=0.87, P<0.001). WSSmean also showed the highest diagnostic performance for detecting ≥70% stenosis (area under the curve, 0.96; 95% confidence interval, 0.92 to 0.99; cutoff, 2.25 Pa), compared with other VFI-derived metrics and RF-ASI. Segmental analysis revealed that WSS values were highest at the plaque peak, whereas turbulence-related metrics were more pronounced in distal segments. In SRU-discordant cases (7 of 90), WSSmean agreed with anatomic imaging–based classification (≥70% vs. <70%) in six of seven lesions.

Conclusion: VFI-derived WSSmean demonstrated the highest diagnostic performance for detecting severe (≥70%) carotid stenosis. In contrast, RF-ASI showed limited discriminatory ability and may primarily reflect global arterial stiffness rather than focal plaque severity.

Keywords: Internal carotid artery; Carotid artery diseases; Ultrasonography; Pulse wave analysis; Hemodynamics

Key points: Mean wall shear stress (WSSmean) at the plaque peak demonstrated the highest diagnostic performance in detecting severe (≥70%) stenosis (area under the curve, 0.96; 95% confidence interval, 0.92 to 0.99; cutoff, 2.25 Pa). Segmental analysis showed that wall shear stress and turbulence parameters were highest at the plaque peak and in distal segments, respectively, indicating spatial heterogeneity in flow patterns. WSSmean may complement conventional ultrasonographic findings in cases of borderline carotid stenosis and in Society of Radiologists in Ultrasound–anatomic imaging–discordant cases, with agreement observed in six of seven discordant lesions.

ORIGINAL ARTICLE

https://doi.org/10.14366/usg.25195
eISSN: 2288-5943
Ultrasonography 2026;45:252-263

Received: September 23, 2025
Revised: January 4, 2026
Accepted: January 5, 2026

Correspondence to:
Nezih Yaylı, MD, Department of Radiology, Bozok University Faculty of Medicine, Capanoğlu, 66100 Azizli/Yozgat, Türkiye
Tel. +90-354-212-7010
Fax. +90-354-212-7010
E-mail: nezihyayli@hotmail.com

This is an Open Access article distributed under the terms of the Creative Commons Attribution Non-Commercial License (http://creativecommons.org/licenses/by-nc/4.0/) which permits unrestricted noncommercial use, distribution, and reproduction in any medium, provided the original work is properly cited.

Copyright © 2026 Korean Society of Ultrasound in Medicine (KSUM)

How to cite this article:
Yaylı N, Karabörk Kılıç AC, Küçük Biçer B, Öncü F, Altıparmak T, Cerit MN, et al. Diagnostic performance of vector flow imaging–derived wall shear stress and radiofrequency echo-tracking-derived arterial stiffness indices in severe carotid stenosis. Ultrasonography 2026 May;45(3):252-263.

Introduction

Ischemic stroke is a leading global health problem and the second most common cause of death and disability [1]. Atherosclerotic carotid artery disease (CAD) accounts for approximately 20% of ischemic strokes and is often clinically silent [2]. While severe stenosis may lead to ischemia due to hypoperfusion, ischemic stroke may also occur in the absence of significant stenosis as a result of plaque rupture and thromboembolism [3]. Although digital subtraction angiography (DSA) is the gold standard for the evaluation of CAD, its invasive nature limits its routine use for diagnostic purposes [4]. The use of contrast media in computed tomography angiography (CTA) and magnetic resonance angiography (MRA) further limits routine application, particularly in patients with renal failure [5,6]. Therefore, ultrasound (US) is widely used as a first-line modality because it is noninvasive and readily available [6]. However, the velocity-based stenosis grading of the Society of Radiologists in Ultrasound (SRU) criteria provides limited information regarding the hemodynamic complexity of CAD [7].

The role of hemodynamic forces in the pathogenesis of atherosclerosis is increasingly being investigated [8]. Through mechanotransduction pathways, hemodynamic forces are converted into biochemical responses within endothelial cells [8,9]. Among these forces, wall shear stress (WSS) is a tangential force exerted by blood flow on the endothelial surface, and altered shear patterns have been implicated in plaque development and vulnerability [9]. Turbulent flow can generate irregular and oscillatory shear forces along the vessel wall, leading to localized mechanical stress that may trigger inflammatory signaling [10,11]. Furthermore, the mechanical properties of the vessel wall interact with intraluminal hemodynamic forces; accordingly, arterial stiffness can influence local flow dynamics by altering wave propagation and wall deformation [12].

Novel US-based techniques, such as vector flow imaging (VFI) and radiofrequency (RF) echo-tracking, have been introduced to evaluate these hemodynamic forces [13–15]. Previous VFI studies have demonstrated a strong correlation between WSS and stenosis severity and have established cutoff values for WSS in the detection of severe carotid stenosis [15,16]. Subsequent work further showed improved diagnostic performance with the incorporation of turbulence-related parameters [17].

Radiofrequency echo-tracking–derived arterial stiffness indices (RF-ASI) have been widely investigated as markers of vascular aging and have shown consistent associations with subclinical atherosclerosis [18,19]. However, despite this growing body of evidence, RF-ASI have not been incorporated into carotid stenosis grading frameworks. Moreover, VFI-derived hemodynamic metrics and RF-ASI have not yet been evaluated concurrently at the plaque level within the same patient cohort.

Therefore, this study was designed with three specific aims. The first aim was to compare the diagnostic performance of VFI-derived hemodynamic parameters and RF-ASI for detecting severe (≥70%) internal carotid artery (ICA) stenosis. The second aim was to determine whether VFI-derived parameters provide complementary hemodynamic information beyond SRU-based stenosis classification. The third aim was to characterize the spatial distribution and interaction patterns of VFI-derived parameters across plaque segments through plaque-based segmental analysis.

Materials and Methods

Compliance with Ethical Standards

This prospective observational study was approved by the institutional ethics committee (approval No. AEŞH-EK1-2024-0021), and written informed consent was obtained from all participants.

Study Design and Patient Selection

Between May and July 2024, a total of 130 consecutive patients with suspected or known CAD who were referred to Department of Radiology, Gazi University Faculty of Medicine for carotid Doppler US were initially screened for eligibility (Fig. 1).

The inclusion criteria were as follows: (1) age ≥18 years and (2)

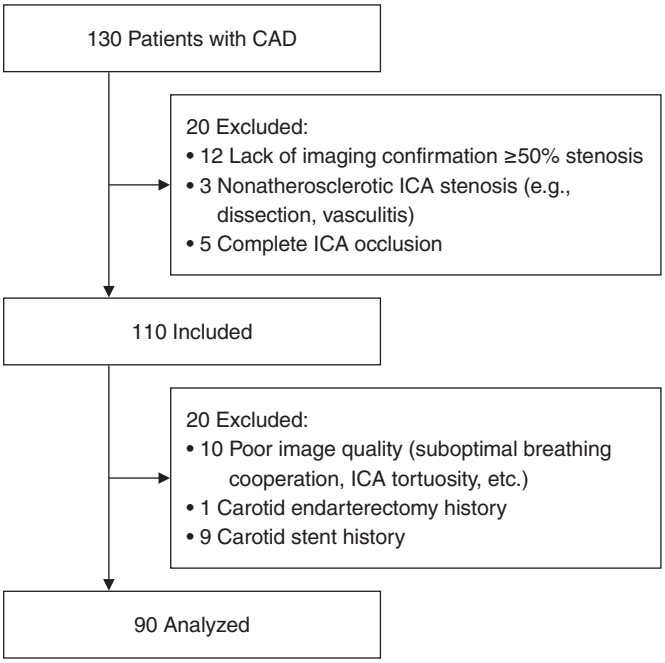


Fig. 1. **Flowchart illustrating patient selection, application of exclusion criteria, and formation of the final study cohort.** CAD, carotid artery disease; ICA, internal carotid artery; N, number of patients.

presence of an atherosclerotic plaque at the carotid bifurcation (bulb/proximal ICA). Carotid stenosis severity was categorized as <50%, 50%–69%, or ≥70% according to the SRU criteria. In patients with ≥50% stenosis, the severity of stenosis was subsequently confirmed using CTA, DSA, or MRA.

The exclusion criteria were as follows: (1) non-atherosclerotic ICA stenosis, such as dissection or vasculitis; (2) complete ICA occlusion; (3) absence of confirmatory imaging (CTA, DSA, or MRA) in patients classified as having ≥50% stenosis on Doppler US; (4) inadequate image quality for Doppler or VFI acquisition resulting from poor breathing cooperation, marked vessel tortuosity, or other technical limitations; and (5) prior carotid endarterectomy or carotid artery stenting.

In total, 90 patients met the eligibility criteria and were included in the final analysis. Demographic and clinical data, including cardiovascular risk factors and history of stroke, were systematically recorded for all participants.

Conventional Carotid Doppler US

All US examinations were performed using a single US system (Mindray Biomedical Electronics Co., Ltd., Shenzhen, China) equipped with an L9-3U (1.8–9.8 MHz) linear array transducer. All examinations were conducted by a single radiologist with 5 years of experience in vascular US to ensure procedural consistency. The common carotid artery (CCA), bifurcation, external carotid artery, and ICA were evaluated using B-mode imaging. Intima–media thickness was measured on longitudinal CCA images, and the arterial lumen was systematically evaluated for the presence of atherosclerotic plaques. Plaque length, thickness, and echogenicity were recorded for each lesion. Plaques were classified using an echogenicity-based scale ranging from predominantly hypoechoic plaques (type 1) to predominantly hyperechoic or calcified plaques (type 5). Initial stenosis grading was performed according to the SRU consensus criteria [7]. At the plaque level, following technical optimization that included angle correction and velocity scale adjustment, Doppler sampling was performed at the visually most stenotic segment identified on combined B-mode and color Doppler imaging. Peak systolic velocity and end-diastolic velocity values were then recorded. In patients with ≥50% stenosis on Doppler US, final stenosis grading was determined using North American Symptomatic Carotid Endarterectomy Trial (NASCET) criteria based on DSA (n=45), CTA (n=10), or MRA (n=5) findings.

VFI and RF Echo-Tracking–Derived Stiffness Indices: Acquisition and Quantitative Analysis

After the Doppler examination, the V-Flow mode was activated. The transducer was positioned in a longitudinal-oblique plane to visualize the stenotic segment, and acquisition parameters were standardized as follows: frequency, 5 MHz; depth, 2–4 cm; arrow life cycle, 25 ms; and arrow density, 10% [16]. A region of interest (ROI) was positioned over the stenotic segment for vector imaging. A high-frame-rate cine loop covering at least one complete cardiac cycle (approximately 2 seconds) was acquired for subsequent quantitative analysis.

After completion of the VFI assessment, the RF echo-tracking mode was activated on the US system. Measurements were obtained at the level of the stenotic plaque. To improve measurement consistency, the probe was aligned as parallel as possible to the vessel axis, and an appropriate ROI was selected. Patients were instructed to briefly hold their breath during image acquisition to minimize motion-related artifacts. Following automated segmentation of the anterior and posterior vessel walls by the system, vessel wall displacement and diameter changes were recorded using cine loops covering at least six cardiac cycles.

Quantitative measurements were performed using the peak systolic phase selected from the high-frame-rate cine loops. WSS analysis was conducted at three predefined plaque segments: proximal (upstream), peak (narrowest), and distal (downstream). ROIs were positioned on the plaque surface and aligned parallel to the local direction of flow. Two ROIs were placed per segment, and mean values of maximum wall shear stress (WSSmax) and mean wall shear stress (WSSmean) were calculated and expressed in pascals (Pa). WSS values were automatically derived by the system using velocity components parallel to the vessel wall and the radial distance from the vessel wall.

Turbulence measurements were obtained using the "Velocity ROI" function, with ROIs placed at the same three plaque segments. The turbulence index (TUR) and time-averaged turbulence (TAT) were automatically calculated based on changes in flow vector direction and magnitude and were reported as percentage values (%) [20]. Higher values reflect increasingly disturbed or complex flow patterns.

For RF echo-tracking analysis, six cardiac cycles in which arterial wall motion was optimally visualized were selected. Systolic and diastolic blood pressure values were entered into the system, after which the hardness coefficient (HC) and pulse wave velocity (PWV, m/s) were automatically calculated based on vessel dilatation, blood pressure data, vessel diameter (Dd), diameter change (ΔD), and pulse pressure (Δp).

All VFI and RF echo-tracking images were jointly reviewed by two radiologists, one with more than 20 years of experience in vascular imaging and the other with 5 years of experience. Image quality, ROI placement, and measured parameter values were reviewed collaboratively. Each measurement was performed three times, and the mean value was used for analysis. Any discrepancies were resolved by consensus.

Statistical Analyses

All statistical analyses were performed using SPSS version 27.0 (IBM Corp., Armonk, NY, USA), and graphical visualizations were generated using Python (v3.10). Continuous variables were expressed as mean ± standard deviation or median (interquartile range), whereas categorical variables were expressed as counts and percentages (n, %). Data normality was assessed using the Shapiro-Wilk test. Comparisons of VFI and RF-ASI parameters among the three stenosis groups (< 50%, 50%–69%, and ≥ 70%) were performed using analysis of variance or the Kruskal-Wallis test, depending on data distribution. Spearman rank correlation analysis was used to assess associations between stenosis severity and imaging parameters, as well as interrelationships among VFI-derived metrics. To assess the diagnostic accuracy of VFI and RF-ASI parameters for detecting ≥ 70% stenosis, receiver operating characteristic (ROC) curve analysis was performed, the area under the curve (AUC) was calculated, and optimal cutoff values were determined using the Youden index. Differences in VFI parameters according to plaque location were evaluated using the paired-samples t-test. A P-value < 0.05 was considered statistically significant.

Table 1. Baseline characteristics of the study population

Variable	Value
Demographics	
Age (year)	70.38 ± 8.7
Male sex	50 (55.6)
Female sex	40 (44.4)
Vascular risk factors and comorbidities	
Hypertension	71 (78.9)
Diabetes mellitus	45 (50.0)
Hyperlipidemia	68 (75.6)
Coronary artery disease	35 (38.9)
Peripheral artery disease	36 (40.0)
History of stroke	37 (41.1)
Smoking status	
Never smoker	38 (42.2)
Former smoker	36 (40.0)
Current smoker	16 (17.8)
Body mass index (kg/m^2)	
< 25.0	23 (25.6)
≥ 25.0	67 (74.4)
Plaque type (echogenicity-based classification)[a]	
Type 1	12 (13.3)
Type 2	9 (10.0)
Type 3	18 (20.0)
Type 4	29 (32.2)
Type 5	22 (24.4)
Stenosis group[b]	
< 50%	30 (33.3)
50%–69%	29 (32.2)
≥ 70%	31 (34.5)

Values are presented as mean±standard deviation or number (%).
[a]Plaque echogenicity types were classified using the echogenicity grading system described in the Materials and Methods section. [b]Stenosis severity classification: ≥50% stenosis was confirmed by the reference standard described in the Materials and Methods section; <50% stenosis was classified using Society of Radiologists in Ultrasound (SRU) criteria.

Results

Patient Characteristics and Descriptive Imaging Findings

The baseline demographic and clinical characteristics of the study population are summarized in Table 1. A total of 90 patients were included in the analysis, with a mean age of 70.4 ± 8.7 years, and 55.6% of the cohort was male. Stenosis severity was classified as < 50% in 33.3% of patients, 50%–69% in 32.2%, and ≥ 70% in 34.5%.

The distribution of VFI-derived parameters across plaque segments, as well as plaque-level RF-ASI parameters, is summarized in Table 2.

Correlation between Parameters and Stenosis Severity

Peak-segment WSSmean showed the strongest correlation with stenosis severity ($r_s = 0.87$, $P < 0.001$). In the distal segment, correlation

Table 2. Descriptive statistics of VFI-derived parameters and RF-ASI parameters

VFI parameter	Value
Plaque proximal	
WSSmax (Pa)	2.16 ± 1.03
WSSmean (Pa)	0.79 ± 0.44
TUR (%)	3.70 ± 7.73
TAT (%)	3.26 ± 5.74
Plaque peak	
WSSmax (Pa)	6.38 ± 3.32
WSSmean (Pa)	2.16 ± 1.03
TUR (%)	29.59 ± 26.71
TAT (%)	13.06 ± 13.66
Plaque distal	
WSSmax (Pa)	3.66 ± 1.88
WSSmean (Pa)	1.34 ± 3.34
TUR (%)	30.79 ± 24.99
TAT (%)	15.46 ± 15.75
RF-ASI parameters	
HC	4.57 ± 2.56
PWV (m/s)	6.95 ± 2.01

Values are presented as mean±standard deviation.
VFI, vector flow imaging; RF-ASI, radiofrequency echo-tracking–derived arterial stiffness indices; WSSmax, maximum wall shear stress; WSSmean, mean wall shear stress; TUR, turbulence index; TAT, time-averaged turbulence; HC, hardness coefficient; PWV, pulse wave velocity.

coefficients were higher for turbulence metrics (TUR/TAT, $r_s = 0.62$–0.66) than for WSS metrics ($r_s = 0.23$–0.25). Plaque-level RF-ASI parameters demonstrated moderate correlations with stenosis severity (PWV, $r_s = 0.46$; HC, $r_s = 0.45$; both $P < 0.001$) (Table 3).

Groupwise Comparison of Novel US Parameters

Fig. 2 demonstrates increasing peak-segment VFI parameter values with increasing stenosis severity, with detailed statistics provided in Supplementary Table 1. All peak-segment VFI metrics differed significantly across stenosis groups (all $P < 0.001$), whereas proximal-segment differences were limited to WSSmax ($P < 0.001$). In the distal segment, turbulence metrics differed significantly across stenosis groups (both $P < 0.001$), whereas between-group differences in WSS metrics were more limited (WSSmax $P = 0.011$, WSSmean $P < 0.05$). RF-ASI parameters also differed across stenosis groups ($P < 0.001$); however, their distributions overlapped substantially between the 50%–69% and ≥70% groups (Fig. 2, Supplementary Table 1).

Representative VFI and RF echo-tracking imaging examples from patients with <50% and ≥70% stenosis are shown in Figs. 3 and 4, respectively.

Diagnostic Performance of Parameters for Detecting ≥70% Stenosis

ROC analyses of peak-segment VFI metrics and plaque-level RF-ASI parameters for detecting ≥70% stenosis are presented in Fig. 5.

As detailed in Table 4, WSSmean demonstrated the highest diagnostic performance for detecting ≥70% stenosis (AUC, 0.96; 95% confidence interval [CI], 0.92 to 0.99; cutoff, 2.25 Pa; sensitivity, 96.8%; specificity, 84.7%; $P < 0.001$). TUR yielded an AUC of 0.84 (95% CI, 0.76 to 0.92), WSSmax an AUC of 0.82 (95% CI, 0.73 to 0.90), and TAT an AUC of 0.82 (95% CI, 0.72 to 0.90) (all $P < 0.001$). PWV and HC showed lower diagnostic performance, with AUC values of 0.69 (95% CI, 0.58 to 0.80) and 0.68 (95% CI, 0.57 to 0.79), respectively (both $P < 0.001$).

Discordant SRU–NASCET Subgroup

SRU-based grading and NASCET-based classification using CTA, DSA, or MRA were discordant in seven of 90 cases (7.8%). Using ROC-derived cutoffs for ≥70% stenosis, WSSmean correctly classified six of seven discordant cases, compared with three of seven for WSSmax, three of seven for TUR and TAT, and two of seven for PWV and HC. In these discordant cases, WSSmean exceeded the cutoff in three of four lesions classified as ≥70% by NASCET but <70% by SRU, and fell below the cutoff in all three lesions classified as ≥70% by SRU but <70% by NASCET. Individual plaque-level values are provided in Supplementary Table 2; findings are descriptive due to the small sample size.

Relationship between Hemodynamic Parameters

At the plaque peak segment, turbulence metrics showed moderate to strong positive correlations with WSS parameters (TUR vs. WSSmax, $r_s = 0.58$; TUR vs. WSSmean, $r_s = 0.55$; TAT vs. WSSmax, $r_s = 0.61$; TAT vs. WSSmean, $r_s = 0.53$; all $P \leq 0.001$). Additional correlations and corresponding scatter plots are provided in Supplementary Table 3 and Supplementary Fig. 1.

Segmental Differences in Hemodynamic Parameters

Segmental comparisons are summarized in Table 5. Peak-segment WSSmax and WSSmean values were higher than both proximal values (both $P < 0.001$) and distal values (WSSmax $P < 0.001$, WSSmean $P < 0.05$). TUR and TAT values were higher in the distal segment than in the proximal segment (both $P < 0.001$).

Correlations between Hemodynamic Parameters and Clinical Variables

Correlations between hemodynamic indices and clinical variables are presented in Supplementary Table 4. RF-ASI parameters showed weak but statistically significant associations with vascular comorbidities.

Table 3. Correlations between segment-specific hemodynamic parameters and carotid artery stenosis severity

Segment/Parameter	rs[a]	P-value
Proximal VFI		
WSSmax	0.87	<0.001
WSSmean	0.06	0.542
TUR (%)	0.16	0.132
TAT (%)	0.14	0.169
Peak VFI		
WSSmax	0.75	<0.001
WSSmean	0.87	<0.001
TUR (%)	0.63	<0.001
TAT (%)	0.61	<0.001
Distal VFI		
WSSmax	0.23	<0.05
WSSmean	0.25	<0.05
TUR (%)	0.62	<0.001
TAT (%)	0.66	<0.001
Plaque RF-ASI		
PWV	0.46	<0.001
HC	0.45	<0.001

VFI, vector flow imaging; WSSmax, maximum wall shear stress; WSSmean, mean wall shear stress; TUR, turbulence index; TAT, time-averaged turbulence; RF-ASI, radiofrequency echo-tracking–derived arterial stiffness indices; PWV, pulse wave velocity; HC, hardness coefficient.
[a]Spearman correlation coefficient.

Discussion

In this study, VFI-derived hemodynamic metrics, particularly peak-segment WSSmean, demonstrated the highest diagnostic performance (AUC, 0.96; 95% CI, 0.92 to 0.99) for identifying severe (≥70%) carotid stenosis when compared with other VFI-derived metrics and RF-ASI. Segmental analyses further indicated spatial heterogeneity in flow-related parameters, characterized by higher WSS values at the plaque peak and more pronounced turbulence in distal segments. In addition, WSSmean provided complementary information in the small subgroup of cases with discordant SRU-based grading and anatomic imaging–based stenosis classification.

Previous studies have investigated VFI-derived WSS metrics in relation to plaque vulnerability, cerebrovascular risk stratification, and stenosis severity assessment [21–25], whereas VFI-based turbulence analyses have more frequently remained qualitative or focused on segmental flow-pattern comparisons [26,27]. Qiu et al. [16] reported excellent diagnostic performance for detecting severe carotid artery stenosis in a VFI-based study (AUC, 0.96 when combined with conventional US). Similarly, Hong et al. [17] demonstrated good diagnostic performance for severe CAD using VFI-derived parameters (TUR, AUC≈0.80; WSSmean, AUC = 0.84). In the present study, overall diagnostic performance for detecting severe CAD was comparable to that reported by Qiu et al. [16]. Moreover, the cutoff values defined for VFI metrics were close to those reported by Hong et al. [17] using a similar US platform (WSSmean, 2.647 Pa; TUR, 22.98%).

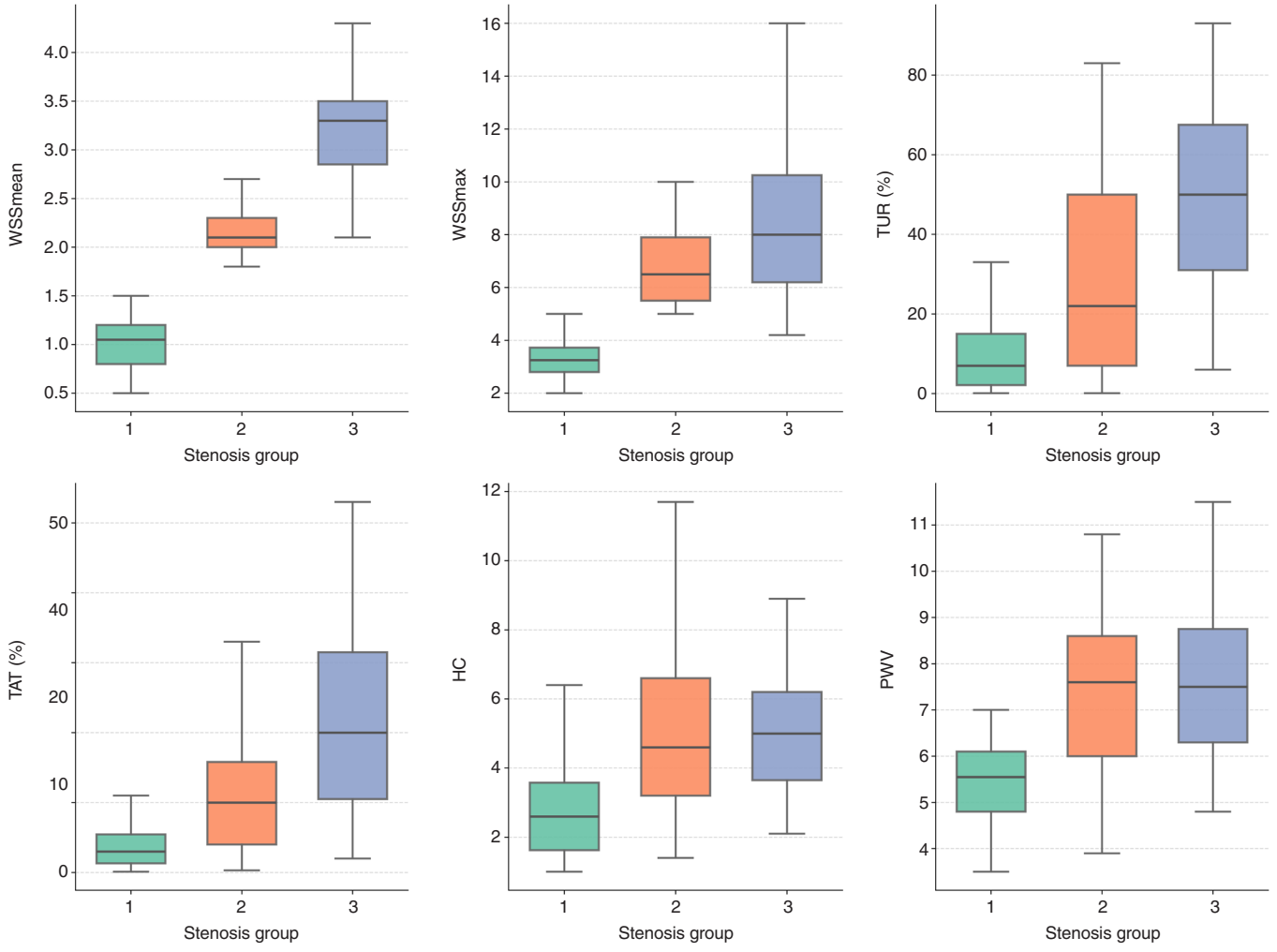


Fig. 2. Boxplots of wall shear stress and arterial stiffness indices measured at the plaque peak level across the three stenosis groups. Patients in group 1 had <50% stenosis, those in group 2 had 50%–69% stenosis, and those in group 3 had ≥70% stenosis. Supplementary Table 1 complements the boxplot visualization by providing detailed medians, interquartile ranges, and P-values for all plaque-level measurements. WSSmean, mean wall shear stress; WSSmax, maximum wall shear stress; TUR, turbulence index; TAT, time-averaged turbulence; HC, hardness coefficient; PWV, pulse wave velocity.

Collectively, variability in reference standards, cohort characteristics, and device or software implementations likely contributes to differences in reported cutoff values and diagnostic performance across studies.

Segment-based distribution patterns of WSS and turbulence parameters across carotid plaques have been described in a limited number of prior studies [28,29]. These studies consistently report the highest WSS at the plaque peak and often describe higher WSS values proximally than distally [29]. In the present cohort, while peak-level findings were concordant with prior reports, WSSmax was higher distally than proximally. This divergence may be attributable to plaque morphology; accordingly, associations between morpho-

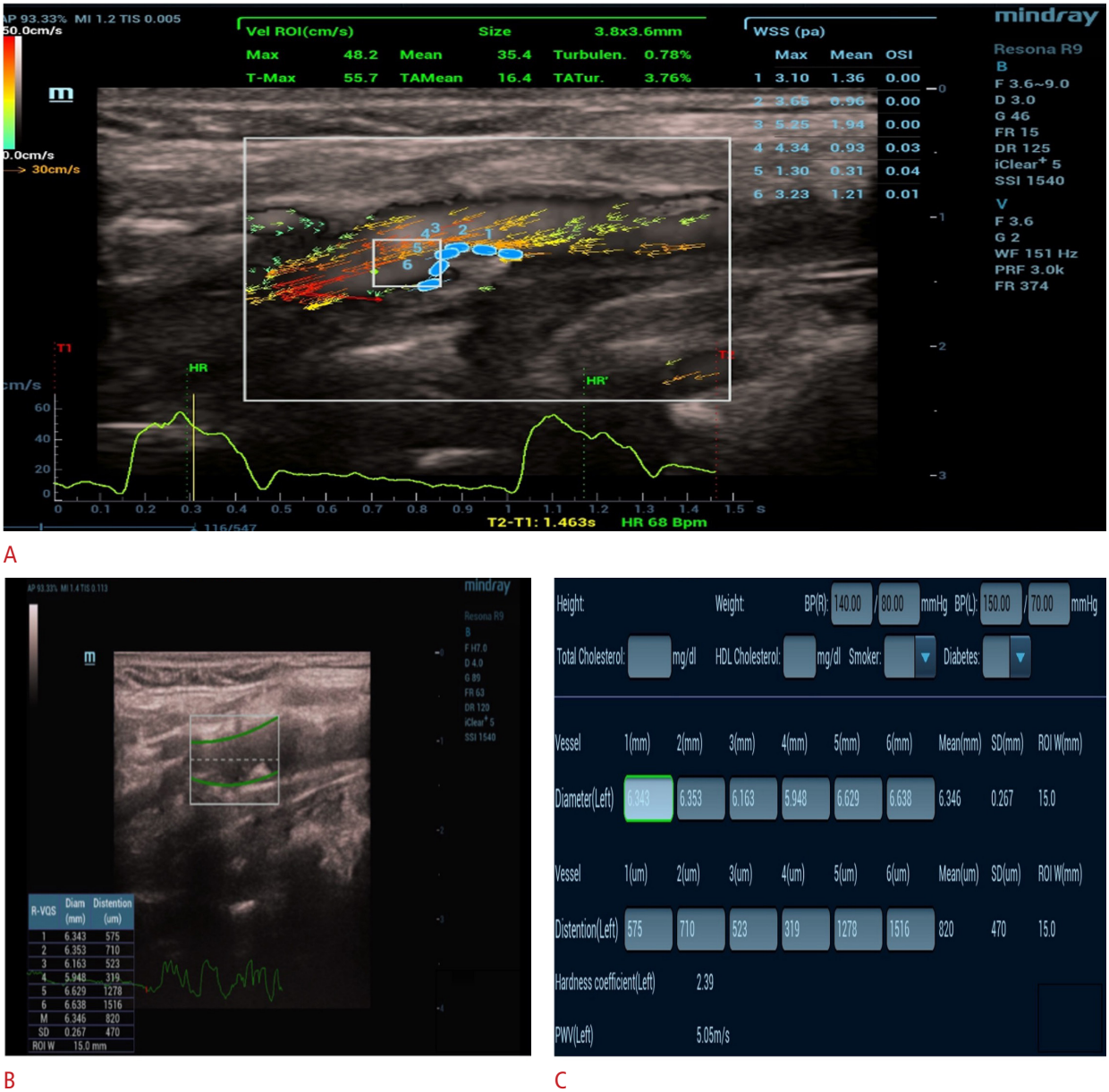
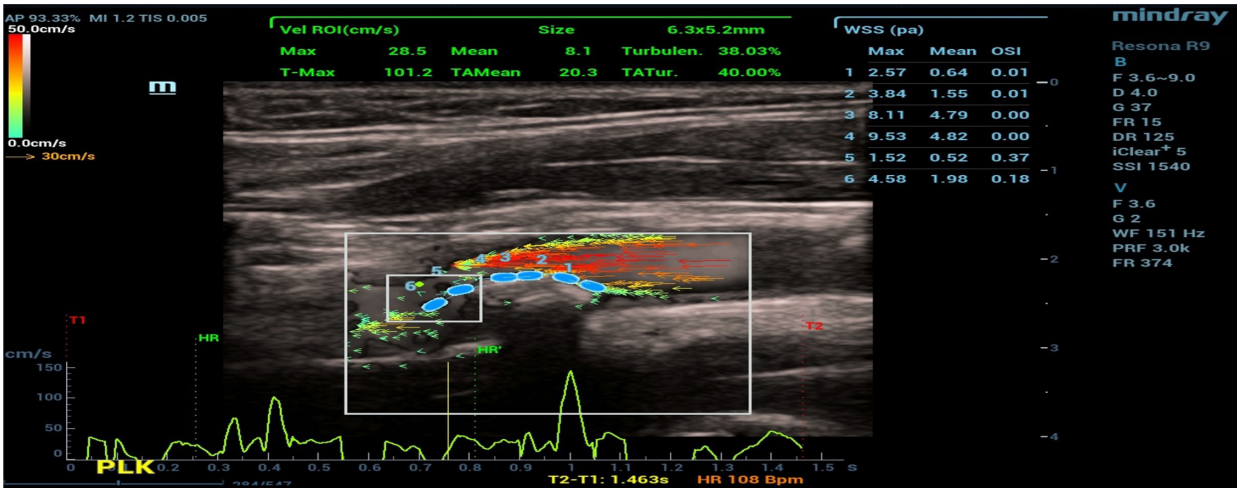
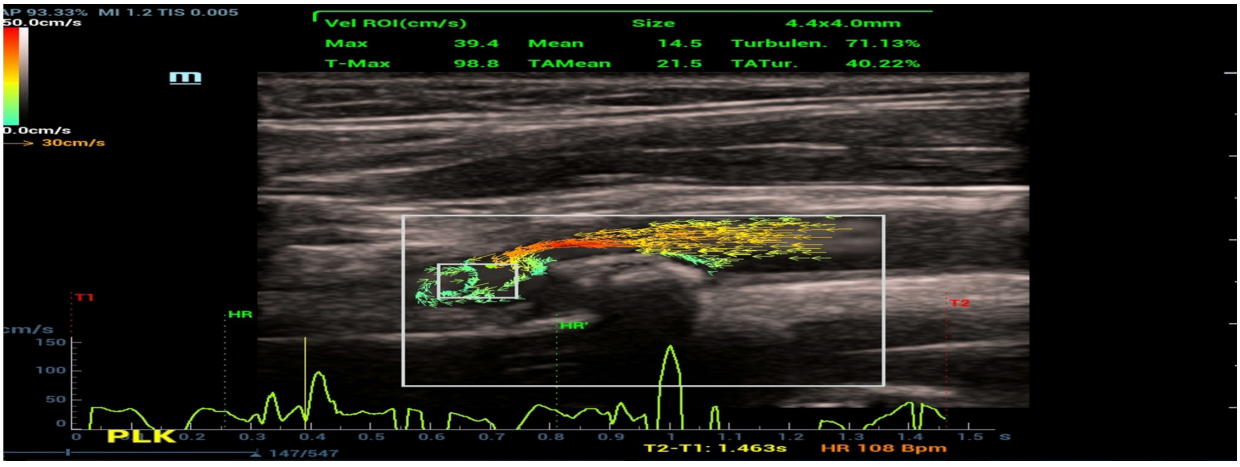


Fig. 3. Representative example of mild carotid artery stenosis (<50%), illustrating plaque-level hemodynamic parameters derived from vector flow imaging (VFI) and arterial stiffness parameters obtained using radiofrequency (RF) echo-tracking.

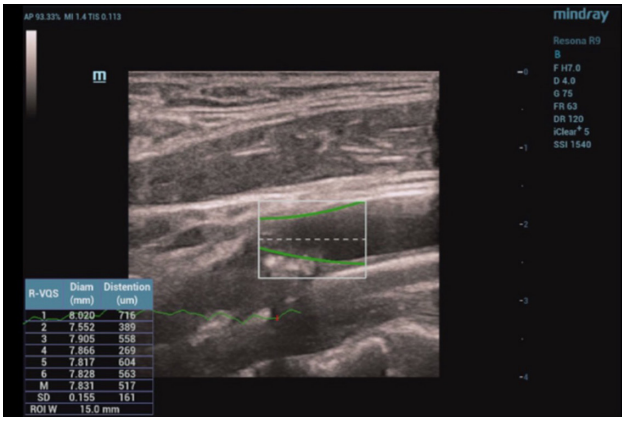
A. VFI analysis shows velocity vector mapping. Short green and yellow vectors indicate relatively low flow velocities (maximum wall shear stress [WSSmax], 4.79 Pa; mean wall shear stress [WSSmean], 1.43 Pa). Regions of interest (ROI) for WSS measurements are placed at the plaque proximal (1–2), peak (3–4), and distal segments (5–6). Turbulence parameters in the distal segments are shown as turbulence index (TUR) 0.78% and time-averaged turbulence (TAT) 3.76%. B, C. RF echo-tracking analysis shows arterial stiffness parameters (pulse wave velocity [PWV], 5.05 m/s; hardness coefficient, 2.39).



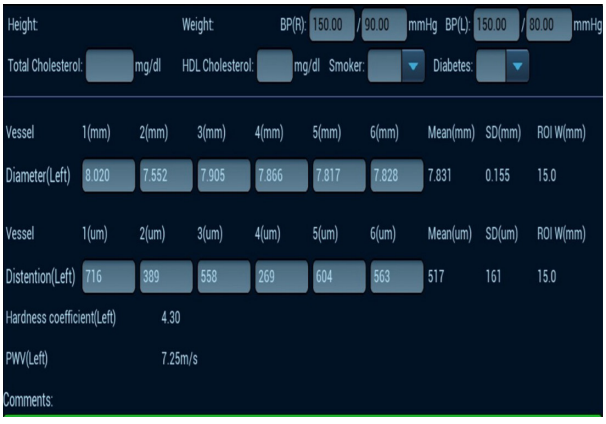
A



B



C



D

Fig. 4. Representative example of severe carotid artery stenosis (≥70%), illustrating plaque-level hemodynamic parameters derived from vector flow imaging (VFI) and arterial stiffness parameters obtained using radiofrequency (RF) echo-tracking.

A. VFI analysis shows velocity vector mapping. Long red vectors indicate markedly increased flow velocities (maximum wall shear stress [WSSmax], 8.82 Pa; mean wall shear stress [WSSmean], 4.80 Pa). Regions of interest for WSS measurements are placed at the proximal (1–2), peak (3–4), and distal segments (5–6) of the plaque. Turbulence parameters in the distal segments are shown as turbulence index (TUR) 38.03% and time-averaged turbulence (TAT) 40%. B. A distinct vortex pattern is observed within the stenotic segment. C, D. RF echo-tracking analysis shows arterial stiffness parameters (pulse wave velocity [PWV], 7.25 m/s; hardness coefficient, 4.30), consistent with increased vessel stiffness.

logical features and segment-based hemodynamic variables were examined (Supplementary Table 5). Plaque thickness and length showed positive correlations with peak- and distal-level hemodynamic parameters, whereas no significant correlations were observed at the proximal segment. Taken together, these morphology–hemodynamics relationships may help explain the relatively higher distal WSSmax observed in this cohort. Nevertheless, these associations should be interpreted cautiously given the correlational design and modest sample size and require confirmation in larger studies. Consistent with prior reports, turbulence metrics were higher distally than proximally [26,27], supporting a distal predominance of flow disturbance.

Previous investigations have also reported a negative correlation between WSS and turbulence parameters, most commonly at the carotid bifurcation level [30]. In contrast, the present analysis demonstrated a moderate to strong positive correlation between these parameters at the plaque peak ($r_s = 0.53–0.61$, $P \leq 0.001$), alongside a weak negative correlation between TAT and WSSmean at the proximal segment ($r_s = -0.21$, $P < 0.05$) (Supplementary Table 3), indicating segment-dependent relationships. This apparent discrepancy may reflect region-specific flow conditions within stenotic plaques, where localized acceleration and flow disturbance coexist [28]. Supporting this interpretation, a similar positive coupling between turbulence-related metrics and WSS has been reported using in vivo four-dimensional magnetic resonance imaging [31]. The observed peak-level WSS–turbulence coupling may therefore represent a high-stress hemodynamic environment, although its prognostic significance remains to be established through longitudinal studies.

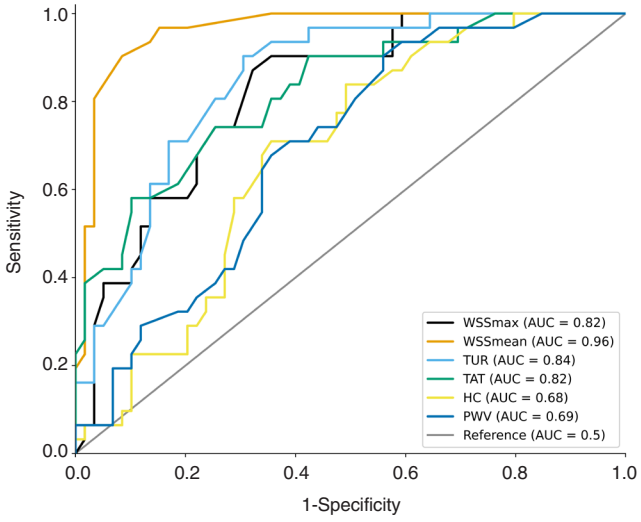


Fig. 5. Receiver operating characteristic curves of plaque peak-level parameters for detecting ≥70% carotid stenosis. Area under the curve (AUC) values are shown in the legend, and the corresponding 95% confidence intervals and optimal cutoff values are provided in Table 4. WSSmax, maximum wall shear stress; WSSmean, mean wall shear stress; TUR, turbulence index; TAT, time-averaged turbulence; HC, hardness coefficient; PWV, pulse wave velocity.

Given its performance in discriminating ≥70% stenosis in this cohort, WSSmean may serve as an adjunct to SRU-based Doppler velocity criteria when classifying stenosis as ≥70% versus <70%. This complementary value was most evident in cases where SRU-based grading and anatomic imaging–based stenosis classification were discordant. Within this discordant subgroup (n=7), WSSmean aligned with the ≥70% versus <70% classification in six of seven lesions, whereas other VFI indices and RF-ASI demonstrated limited agreement. Specifically, WSSmean exceeded the ROC-derived cutoff in lesions classified as ≥70% by anatomic imaging but <70% by SRU and fell below the cutoff in the reverse discordant scenario (SRU ≥70% and anatomic imaging <70%). Although this analysis is descriptive and based on a small number of cases, it suggests that WSSmean may provide additional support when distinguishing borderline 50%–69% from ≥70% stenosis in discordant assessments.

RF-ASI have primarily been studied as markers of systemic vascular involvement at the CCA level, and their utility in classifying focal plaque-level stenosis has not been systematically examined [18,19]. In this cohort, plaque-level PWV and HC demonstrated lower discriminatory performance than VFI-derived hemodynamic metrics, suggesting that these indices may more accurately reflect a general-

Table 4. ROC analysis results for detecting ≥70% carotid artery stenosis

Parameter	AUC (95% CI)	Cutoff	P-value[a]	Sensitivity (%)	Specificity (%)
WSSmean (Pa)	0.96 (0.92–0.99)	2.25	<0.001	96.8	84.7
WSSmax (Pa)	0.82 (0.73–0.90)	6.4	<0.001	74.2	74.6
TUR (%)	0.84 (0.76–0.92)	29.5	<0.001	80.6	74.6
TAT (%)	0.82 (0.72–0.90)	11.5	<0.001	74.2	74.6
HC	0.68 (0.57–0.79)	4.35	<0.001	67.7	66.1
PWV (m/s)	0.69 (0.58–0.80)	7.1	<0.001	67.7	64.4

ROC, receiver operating characteristic; AUC, area under the curve; CI, confidence interval; WSSmean, mean wall shear stress; WSSmax, maximum wall shear stress; TUR, turbulence index; TAT, time-averaged turbulence; HC, hardness coefficient; PWV, pulse wave velocity.
[a]P-values are for testing whether the AUC is significantly different from 0.5.

Table 5. Segmental comparisons of VFI-derived parameters

Comparison	Parameter	Mean difference (95% CI)	t-value[a]	P-value
Plaque proximal–plaque peak level	WSSmax	–3.25 (–3.92 to –2.57)	–9.56	< 0.001
	WSSmean	–1.37 (–1.58 to –1.16)	–12.95	< 0.001
	TUR (%)	–25.89 (–31.56 to –20.21)	–9.07	< 0.001
	TAT (%)	–9.79 (–12.76 to –6.80)	–6.53	< 0.001
Plaque peak–plaque distal level	WSSmax	2.71 (2.02 to 3.40)	7.83	< 0.001
	WSSmean	0.82 (0.14 to 1.50)	2.39	< 0.05
	TUR (%)	–1.19 (–6.57 to 4.18)	–0.44	0.662
	TAT (%)	–2.40 (–5.52 to 0.72)	–1.52	0.128
Plaque proximal–plaque distal level	WSSmax	–0.53 (–0.94 to –0.12)	–2.56	< 0.05
	WSSmean	–0.54 (–1.23 to 0.14)	–1.56	0.121
	TUR (%)	–27.08 (–32.12 to –22.04)	–10.68	< 0.001
	TAT (%)	–12.19 (–15.57 to –8.80)	–7.16	< 0.001

VFI, vector flow imaging; CI, confidence interval; WSSmax, maximum wall shear stress; WSSmean, mean wall shear stress; TUR, turbulence index; TAT, time-averaged turbulence.
[a]t values were derived from the paired-samples t-test.

ized arterial stiffness phenotype rather than focal luminal stenosis severity. PWV and HC showed weak but statistically significant associations with markers of systemic atherosclerotic burden, including peripheral artery disease, coronary artery disease, and hypertension (Supplementary Table 4). However, these associations should be interpreted cautiously in the absence of multivariable adjustment.

This study has several limitations. First, the sample size was modest and derived from a single center, underscoring the need for multicenter validation in more diverse populations. Second, VFI-derived metrics and RF-ASI are dependent on platform and software implementation; accordingly, the cutoff values reported here should be regarded as device- and protocol-specific and require external validation or recalibration across systems. Third, plaque-level RF-ASI measurements are susceptible to motion-related artifacts and local geometric factors, including respiratory or cardiac motion, vessel tortuosity, and plaque or wall heterogeneity. Additionally, formal inter- or intra-observer reproducibility analyses were not performed, which may have contributed to the lower performance of PWV and HC in plaque-level stenosis classification. Improved software support for standardized plaque-level ROI definition, including manual correction when necessary, may enhance reproducibility and should be explored in future studies. Finally, partial verification bias cannot be excluded, particularly in the low-grade stenosis group. In this cohort, arteries with SRU-based stenosis ≥50% underwent NASCET-based assessment using CTA, MRA, or DSA as the reference standard for ROC analyses of ≥70% stenosis, whereas arteries with SRU <50% did not undergo systematic anatomic imaging [32]. Although duplex US has good accuracy for detecting 0%–49% stenosis [5], the absence of a uniform anatomic reference in the <50% group may result in overestimation of specificity and AUC. Consequently, the diagnostic performance of WSSmean should be interpreted with caution, and future prospective studies applying a uniform anatomic imaging reference across all stenosis categories are warranted.

In summary, VFI-derived WSSmean emerged as the strongest ultrasonographic parameter for identifying severe (≥70%) carotid artery stenosis. Segmental VFI analysis revealed spatial heterogeneity in hemodynamic patterns, with higher WSS at the plaque peak and more pronounced turbulence in distal segments. In contrast, RF-ASI parameters, including PWV and HC, demonstrated limited added value for distinguishing severe stenosis relative to VFI-derived metrics. Importantly, WSSmean may provide complementary information in cases where SRU-based Doppler grading and NASCET-based stenosis classification are discordant.

ORCID

Nezih Yaylı: https://orcid.org/0000-0002-0988-029X
Atiye Cenay Karabörk Kılıç: https://orcid.org/0000-0002-9980-8397
Burcu Küçük Biçer: https://orcid.org/0000-0002-5615-264X
Fatih Öncü: https://orcid.org/0000-0003-1673-7253
Taylan Altıparmak: https://orcid.org/0000-0002-8803-8542
Mahi Nur Cerit: https://orcid.org/0000-0003-2878-6052
Halit Nahit Şendur: https://orcid.org/0000-0003-1690-2538
Hale Zeynep Batur Çağlayan: https://orcid.org/0000-0002-3279-1842
Mehmet Koray Akkan: https://orcid.org/0000-0002-1186-1258
Hüseyin Koray Kılıç: https://orcid.org/0000-0002-0718-0097
Suna Özhan Oktar: https://orcid.org/0000-0003-0112-9992
Ahmet Baran Önal: https://orcid.org/0000-0002-2830-3068
Bijen Nazlıel: https://orcid.org/0000-0002-6148-3814
Erhan Turgut Ilgıt: https://orcid.org/0000-0002-2956-6572

Author Contributions

Conceptualization: Yaylı N, Karabörk Kılıç AC, Küçük Biçer B, Öncü F, Al-

tıparmak T, Cerit MN, Şendur HN, Batur Çağlayan HZ, Akkan MK, Kılıç HK, Oktar SÖ, Önal AB, Nazlıel B, Ilgıt ET. Data acquisition: Yaylı N, Karabörk Kılıç AC, Cerit MN, Oktar SÖ, Ilgıt ET. Data analysis or interpretation: Yaylı N, Karabörk Kılıç AC, Küçük Biçer B. Drafting of the manuscript: Yaylı N, Karabörk Kılıç AC, Küçük Biçer B, Öncü F, Altıparmak T, Cerit MN, Şendur HN, Batur Çağlayan HZ, Akkan MK, Kılıç HK, Oktar SÖ, Önal AB, Nazlıel B, Ilgıt ET. Critical revision of the manuscript: Yaylı N. Approval of the final version of the manuscript: all authors.

Conflict of Interest

No potential conflict of interest relevant to this article was reported.

Acknowledgments

The authors are grateful to Mindray for their support regarding the Resona R9 scanner utilized in this study. The authors would also like to thank Dr. Burcu Küçük Biçer for her valuable contribution to the statistical analysis of the study.

Supplementary Material

Supplementary Table 1. Segmental VFI-derived parameters and RF-ASI parameters across stenosis severity groups (https://doi.org/10.14366/usg.25195).

Supplementary Table 2. Plaque-level VFI-derived parameters and RF-ASI parameters in patients with discordant SRU and NASCET stenosis grading (https://doi.org/10.14366/usg.25195).

Supplementary Table 3. Correlations between WSS and turbulence parameters by plaque segment (https://doi.org/10.14366/usg.25195).

Supplementary Table 4. Correlations of VFI-derived parameters and RF-ASI parameters with clinical/cardiovascular characteristics (https://doi.org/10.14366/usg.25195).

Supplementary Table 5. Correlations between plaque morphology and segment-specific hemodynamic parameters (https://doi.org/10.14366/usg.25195).

Supplementary Fig. 1. Scatter plots showing the correlations between peak-level wall shear stress parameters and turbulence parameters in carotid plaques (https://doi.org/10.14366/usg.25195).

References

1. Saini V, Guada L, Yavagal DR. Global epidemiology of stroke and access to acute ischemic stroke interventions. Neurology 2021;97(20 Suppl 2):S6-S16.
2. Song P, Fang Z, Wang H, Cai Y, Rahimi K, Zhu Y, et al. Global and regional prevalence, burden, and risk factors for carotid atherosclerosis: a systematic review, meta-analysis, and modelling study. Lancet Glob Health 2020;8:e721-e729.
3. Homburg PJ, Rozie S, van Gils MJ, Jansen T, de Weert TT, Dippel DW, et al. Atherosclerotic plaque ulceration in the symptomatic internal carotid artery is associated with nonlacunar ischemic stroke. Stroke 2010;41:1151-1156.
4. Bladin CF, Colchester AC, Hawkes DJ, Seifalian AM, Iqbal N, Hardingham CR. Morphological and hemodynamic assessments of carotid stenosis using quantitative digital subtraction angiography. Stroke 1996;27:1672-1678.
5. Chappell FM, Wardlaw JM, Young GR, Gillard JH, Roditi GH, Yip B, et al. Carotid artery stenosis: accuracy of noninvasive tests: individual patient data meta-analysis. Radiology 2009;251:493-502.
6. Wardlaw JM, Chappell FM, Best JJ, Wartolowska K, Berry E. Non-invasive imaging compared with intra-arterial angiography in the diagnosis of symptomatic carotid stenosis: a meta-analysis. Lancet 2006;367:1503-1512.
7. Grant EG, Benson CB, Moneta GL, Alexandrov AV, Baker JD, Bluth EI, et al. Carotid artery stenosis: gray-scale and Doppler US diagnosis: Society of Radiologists in ultrasound consensus conference. Radiology 2003;229:340-346.
8. Hahn C, Schwartz MA. Mechanotransduction in vascular physiology and atherogenesis. Nat Rev Mol Cell Biol 2009;10:53-62.
9. Chiu JJ, Usami S, Chien S. Vascular endothelial responses to altered shear stress: pathologic implications for atherosclerosis. Ann Med 2009;41:19-28.
10. Gessner FB. Brief reviews: hemodynamic theories of atherogenesis. Circ Res 1973;33:259-266.
11. Huveneers S, Daemen MJ, Hordijk PL. Between Rho(k) and a hard place: the relation between vessel wall stiffness, endothelial contractility, and cardiovascular disease. Circ Res 2015;116:895-908.
12. Kim HL, Kim SH. Pulse wave velocity in atherosclerosis. Front Cardiovasc Med 2019;6:41.
13. Li ZJ, Liu Y, Du LF, Luo XH. Evaluating arterial stiffness in type 2 diabetes patients using ultrasonic radiofrequency. J Huazhong Univ Sci Technolog Med Sci 2016;36:442-448.
14. Du Y, Goddi A, Bortolotto C, Shen Y, Dell'Era A, Calliada F, et al. Wall shear stress measurements based on ultrasound vector flow imaging: theoretical studies and clinical examples. J Ultrasound Med 2020;39:1649-1664.
15. Qiu Y, Dong Y, Mao F, Zhang Q, Yang D, Chen K, et al. High-frame rate vector flow imaging technique: initial application in evaluating the hemodynamic changes of carotid stenosis caused by atherosclerosis. Front Cardiovasc Med 2021;8:617391.

16. Qiu YJ, Cheng J, Zhang Q, Yang DH, Zuo D, Mao F, et al. Clinical application of high-frame-rate vector flow imaging in evaluation of carotid atherosclerotic stenosis. Diagnostics (Basel) 2023;13:519.
17. Hong S, Dong Y, Gao W, Song D, Liu M, Li W, et al. Evaluation of carotid stenosis in a high-stroke-risk population by hemodynamic dual-parameters based on ultrasound vector flow imaging. Brain Behav 2024;14:e70150.
18. Jiang X, Ge W, Huang H, Li Y, Liu X, Pang H, et al. Arterial stiffness in subclinical atherosclerosis quantified with ultrafast pulse wave velocity measurements: a comparison with a healthy population using propensity score matching. Ultrasonography 2024;43:263-271.
19. Chang C, Gan L, Liao X, Peng Y, Yang F, Liu W, et al. Quantitative analysis on vessel stiffness and vector flow imaging in the assessment of carotid artery structural and functional changes in patients with type 2 diabetes. Ultrasound Med Biol 2025;51:85-93.
20. Dong Y, Gao W, Hong S, Song D, Liu M, Du Y, et al. Evaluation of turbulence index and flow pattern for atherosclerotic carotid stenosis: a high-frame-rate vector flow imaging study. Ultrasound Med Biol 2024;50:549-556.
21. Zhang X, Ding H, Ji X, Chen L, Huang P, Lin Z, et al. Predicting vulnerable carotid plaques by detecting wall shear stress based on ultrasonic vector flow imaging. J Vasc Surg 2024;80:1475-1486.
22. Papaioannou TG, Karatzis EN, Vavuranakis M, Lekakis JP, Stefanadis C. Assessment of vascular wall shear stress and implications for atherosclerotic disease. Int J Cardiol 2006;113:12-18.
23. Zhou M, Yu Y, Chen R, Liu X, Hu Y, Ma Z, et al. Wall shear stress and its role in atherosclerosis. Front Cardiovasc Med 2023;10:1083547.
24. Malek AM, Alper SL, Izumo S. Hemodynamic shear stress and its role in atherosclerosis. JAMA 1999;282:2035-2042.
25. Zhao M, Chen J, Gu S, Hu H, Zhang L, Wu R, et al. Plaque biomarkers from high-frame rate vector flow imaging and shear wave elastography in mild carotid stenosis. Ultrasonography 2025;44:274-284.
26. Hong S, Dong Y, Song D, Liu M, Gao W, Li W, et al. Precise evaluation of blood flow patterns in human carotid bifurcation based on high-frame-rate vector flow imaging. J Clin Ultrasound 2023;51:1070-1077.
27. Dong Y, Hong S, Song D, Liu M, Gao W, Du Y, et al. Blood flow turbulence quantification of carotid artery with a high-frame rate vector flow imaging. J Ultrasound Med 2023;42:427-436.
28. Goudot G, Poree J, Pedreira O, Khider L, Julia P, Alsac JM, et al. Wall shear stress measurement by Ultrafast vector flow imaging for atherosclerotic carotid stenosis. Ultraschall Med 2021;42:297-305.
29. Chen J, Zhang L, Gu S, Jia C, Wu R. Quantitative evaluation using carotid ultrasonography-based high-frame-rate vector flow imaging in patients with low carotid stenosis. Br J Radiol 2024;97:1476-1482.
30. Song D, Liu M, Dong Y, Hong S, Chen M, Du Y, et al. Investigation on the differences of hemodynamics in normal common carotid, subclavian, and common femoral arteries using the vector flow technique. Front Cardiovasc Med 2022;9:956023.
31. Ziegler M, Alfraeus J, Good E, Engvall J, de Muinck E, Dyverfeldt P. Exploring the relationships between hemodynamic stresses in the carotid arteries. Front Cardiovasc Med 2020;7:617755.
32. Naylor R, Rantner B, Ancetti S, de Borst GJ, De Carlo M, Halliday A, et al. Editor's choice: European Society for Vascular Surgery (ESVS) 2023 clinical practice guidelines on the management of atherosclerotic carotid and vertebral artery disease. Eur J Vasc Endovasc Surg 2023;65:7-111.